Subcritical dynamo bifurcation in the Taylor Green flow

Yannick Ponty, Jean-Phillipe Laval, Bérengère Dubrulle, François Daviaud, Jean-François Pinton

Subcritical dynamo bifurcation in the Taylor Green flow

Y. Ponty[1], J.-P. Laval[2], B. Dubrulle[3], F. Daviaud[3], J.-F. Pinton[4]
[1] *Laboratoire Cassiopée, CNRS UMR6202, Observatoire de la Côte d'Azur, BP 4229, Nice Cedex 04, France*
[2] *Laboratoire de Mécanique de Lille, CNRS UMR8107, Bd P. Langevin, 59655 Villeneuve d'Asq, France*
[3] *Service de Physique de l'Etat Condensé, CNRS URA 2464, CEA Saclay, 91191 Gif-sur-Yvette, France*
[4] *Laboratoire de Physique, de l'École Normale Supérieure de Lyon, CNRS UMR5672, 46 Allée d'Italie, 69007 Lyon, France*

We report direct numerical simulations of dynamo generation for flow generated using a Taylor-Green forcing. We find that the bifurcation is subcritical, and show its bifurcation diagram. We connect the associated hysteretic behavior with hydrodynamics changes induced by the action of the Lorentz force. We show the geometry of the dynamo magnetic field and discuss how the dynamo transition can be induced when an external field is applied to the flow.

PACS numbers: 47.65.-d,91.25.Cw

Larmor [1] is generally credited for suggesting that the magnetic field of the Sun (and, by extension, that of planets and other celestial bodies) could be due to dynamo action – *i.e.* self-generation from the motions of an electrically conducting fluid. This principle has received much theoretical support [2] since then and has recently been validated by experimental observations [3, 4, 5, 6]. Dynamo action results from an instability: when the flow magnetic Reynolds number R_M exceeds a critical value R_M^c, the null magnetic field state looses its stability to a non-zero magnetic field state. Because of the low value the magnetic Prandtl number of the considered fluids, this instability usually happens on a turbulent (noisy) basic state and the choice of an order parameter can be ambiguous [7]. However, we can assume that the usual concepts of stability theory apply (cf. later) and study if the transition is supercritical or subcritical [8]. In most models and in all experiments, this bifurcation is supercritical: R_M^c is a unique number, albeit flow dependant. For instance $R_M^c \sim 14$ and $R_M^c \sim 18$ for the constrained Karlsruhe and Riga experiments, while $R_M^c \sim 32$ for the fully turbulent VKS dynamo [5]. On the other hand, the dynamo bifurcation may also be subcritical particularly because the action of a growing magnetic field is supposed to reduce hydrodynamic turbulence and maintain dynamo action for lower R_M values. In fact, the transition can be globally subcritical if the basic state experiences instability with respect to finite amplitude perturbations [9]. A characteristic hysteretic behavior is then associated to the bifurcation, and the dynamo operates for a range of lower values $R_M^g < R_M < R_M^c$. Subcriticality has been discussed in MHD Alpha-Omega dynamical systems [10, 11] and also for numerical simulations of convective dynamos in spherical geometries [12]

In this Letter, we study the dynamo bifurcation using full MHD simulations, generated in a 3D-periodical domain, by the Taylor Green forcing [13]. At low Reynolds numbers, this flow has several metastable hydrodynamics states [14]. At higher Reynolds numbers, it has a well defined mean flow structure with superimposed intense turbulent fluctuations. Recent studies of the linear problem have shown that, while the dynamo thresholds may runaway in flows generated by random forcing [15], a dynamo is observed at all kinetic Reynolds numbers [16, 17, 18] in the Taylor-Green flow. We study the fully nonlinear regime and report here evidence of the subcriticality of the bifurcation.

Using standard direct numerical simulation (DNS) procedures we integrate pseudospectrally the MHD equations in a 2π-periodic box:

$$\frac{\partial \mathbf{v}}{\partial t} + \mathbf{v}\cdot\nabla\mathbf{v} = -\nabla\mathcal{P} + \mathbf{j}\times\mathbf{B} + \nu\nabla^2\mathbf{v} + \mathbf{F}, \quad (1)$$

$$\frac{\partial \mathbf{B}}{\partial t} + \mathbf{v}\cdot\nabla\mathbf{B} = \mathbf{B}\cdot\nabla\mathbf{v} + \eta\nabla^2\mathbf{B}\ , \quad (2)$$

together with $\nabla\cdot\mathbf{v} = \nabla\cdot\mathbf{B} = 0$; a constant mass density $\rho = 1$ is assumed. Here, $\mathbf{v}$ stands for the velocity field, $\mathbf{B}$ the magnetic field (in units of Alfvén velocity), $\mathbf{j} = (\nabla\times\mathbf{B})/\mu_0$ the current density, ν the kinematic viscosity, η the magnetic diffusivity and $\mathcal{P}$ is the pressure. The forcing term $\mathbf{F}$ is given by the TG vortex

$$\mathbf{F}_{\rm TG}(k_0) = 2f(t)\begin{bmatrix}\sin(k_0\ x)\cos(k_0\ y)\cos(k_0\ z)\\ -\cos(k_0\ x)\sin(k_0\ y)\cos(k_0\ z)\\ 0\end{bmatrix}, \quad (3)$$

implemented here at $k_0 = 1$. In the sequel, we consider two types of forcing: one in which $f(t)$ is set to a constant – this is the constant force forcing ($f(t) = 1.5$) considered in [16]. In a second one $2f(t)$ is set by the condition that the $(1, 1, 1)$ Fourier components of the velocity remains equal to the Taylor-Green vortex – this is the constant velocity forcing considered in [17]. For the linear instability problem, both forcing yield the same value of R_M^c [16, 17]. We now explore the non-linear regime, as well as the response to finite amplitude perturbations. Three control parameters drive the instability: the magnetic and kinetic Reynolds numbers and the amplitude

of an external magnetic field B_0 when applied.

$$R_M = \frac{v^0_{\rm rms}\pi}{\eta} \quad R_V = \frac{v^0_{\rm rms}\pi}{\nu} \quad \Lambda = \frac{B_0}{v^0_{\rm rms}} \ . \qquad (4)$$

In the definition of the Reynolds numbers, the characteristic length scale is set to π, the size of a TG cell when $k_0 = 1$. The characteristic speed $v^0_{\rm rms}$ is computed from hydrodynamic runs in which the Navier-Stokes equation is not coupled to the induction equation, $v^0_{\rm rms} = \langle\sqrt{2E_V(t)}\rangle_t$. Here E_V is net kinetic energy $E_V(t)$ and $\langle\cdot\rangle_t$ stands for averaging in time $(1/T \int^T \cdot\, dt)$. Likewise, in dynamo runs, the intensity of the magnetic field is estimated from the net magnetic energy $E_M(t)$, as $b = \langle\sqrt{2E_M(t)}\rangle_t$.

Previous works [17, 18] have explored the response of TG flows to infinitesimal magnetic perturbations, as a function of the kinetic Reynolds number R_V. It was found that at any R_V, there exists a critical R^c_M above which perturbations grow exponentially. This is illustrated in Fig. 1 for a run at $R_V = 563$ and $R_M = 281$ above the critical value $R^c_M = 206$. The initial magnetic field perturbation – with an energy level $E_M = 10^{-17}$ – first grows exponentially. At time $t \sim 300$, the magnetic field has reached sufficient amplitude so that it can react back onto the velocity field, saturate the instability and reach a statistically stationary state, with approximate equipartition $E_M \sim E_V$. Note that times are given here in units of equation (1), for which 1 is very close to one eddy turnover time of the flow ($T_{\rm NL} = \pi/v^0_{\rm rms} \sim 1.17$). This transition from infinitesimal perturbations builds the (solid) red curve in Fig.2.

We have then quenched the system: at $t = 1000$, the magnetic diffusivity η is suddenly increased by a factor of 4, lowering R_M below R^c_M. After a short transient, both E_V and E_M decrease and reach a second statistically stationary state, with a non zero magnetic energy – a new dynamo state, for which equipartition is reached again (Fig. 1). This behavior is an evidence for global subcriticality [9]. The different levels of fluctuations in the two regimes suggest the possibility of different dynamo states, depending on the magnetic field or on history of the system.

As subcritical bifurcations are also associated with hysteresis cycles, we have repeated the quenching procedure starting from the same dynamo state A (obtained at $t = 1000$ at $R_V = 563$ in Fig. 1) for increasing values of η, i.e. for *decreasing* R_M values. The (time-averaged) magnetic and kinetic energy obtained after rearrangements are then recorded, and results summarized in Fig. 2 by the curve in the $B_0 = 0$ plane. Starting from point A, one can sustain the dynamo after quenching through points $A2$ to $A9$, until a value R^g_M substantially lower than R^c_M (at $A9$, $R_M = 70$ compared to $R_M = 211$ in $A3$).

We have investigated further the system behaviour along the cycle by monitoring the spatial structure of

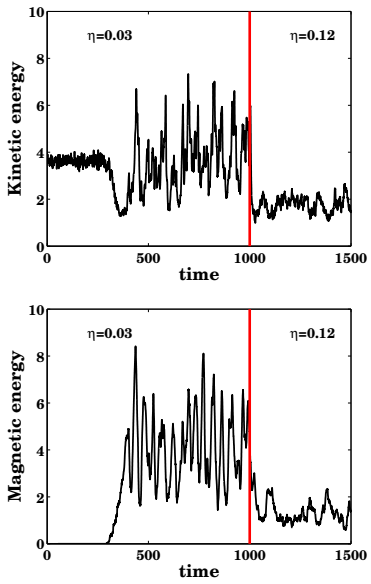

FIG. 1: After a dynamo is self-generated from infinitesimal perturbations, the induction equation is quenched at $t = 1000$ by a four-fold increase of the magnetic diffusivity. It corresponds to a sudden change from A to A_9 – cf. Table I.

Point	η	R_M	b	L_B	$v_{\rm rms}$	L_U
A	0.03	281	2.8	5.2	2.7	3.0
$A2$	0.035	241	2.8	5.3	2.5	3.0
$A3$	0.04	211	2.8	5.4	2.5	2.9
$A4$	0.05	169	2.7	5.5	2.3	2.9
$A5$	0.07	121	2.6	5.7	2.0	2.9
$A6$	0.08	106	2.5	5.7	1.8	2.9
$A7$	0.09	94	2.4	5.7	1.7	2.9
$A8$	0.1	84	2.0	5.5	1.7	2.9
$A9$	0.12	70	1.6	5.1	1.9	3.0
$A10$	0.15	56	0.0	0.0	2.7	2.6

TABLE I: For each regime: root mean square amplitude of the magnetic/*resp.*velocity fields $b = \langle\sqrt{2Em(t)}\rangle$, $v_{\rm rms} = \langle\sqrt{2Ev(t)}\rangle$, integral scale of the magnetic/*resp.*velocity fields $L_B = \langle\sum E_B(k,t))/k\rangle$, $L_U = \langle\sum E_V(k,t))/k\rangle$ – $E(k,t)$ is the uni-dimensional energy spectra.

the magnetic and kinetic energies, so as to detect possible changes in the flow structure. In a first regime, until point $A7$, the kinetic energy (and hence $v_{\rm rms}$, i.e. the turbulence intensity – see Table I) decreases and so does the magnetic energy – equipartition being essentially preserved. Past $A8$, changes occur: E_V starts to increase abruptly, while E_M continues to decrease, resulting in a decreasing ratio E_M/E_V – see also Fig.4. Other global quantities are also changing along this branch (see Table I). It corresponds to a modification in the spatial structure of the magnetic energy. As can bee seen in Fig. 3, the dynamo modes in $A7$ and $A8$ are different. At $A7$,

the dynamo has a structure with magnetic energy 'tubes' in which the field line are concentrated along diagonal direction (aligned with the energy structures). In $A8$, the dynamo has a magnetic energy with a wavy shape and the field line are no longer parallel to the energy structures. In fact, the geometry of the $A8$ and $A9$ dynamo modes is reminiscent of the low kinematic mode of the TG dynamo[18].

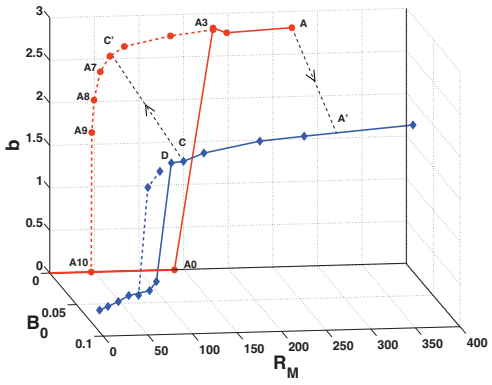

FIG. 2: Bifurcation curves and hysteresis cycles when an external magnetic field is applied (full diamond symbols) or without one (full circle symbols). In this case, the subcritical quenched states (see text) form the red line. Jumps between the two branches link A to A' and C to C'.

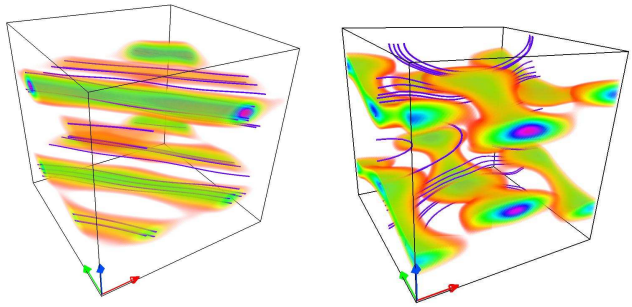

FIG. 3: Volume rendering (75% of max(b)) of the magnetic energy and magnetic field lines [19], for the normalized magnetic field $\langle B(\mathbf{x},t)/B(t)\rangle$ averaged in time during the run; (left) point $A7$ and (right) point $A8$.

As turbulence influences the dynamo, we have repeated the above sequence of quenching at varying kinetic Reynolds numbers R_V. The result is shown in Fig. 4. We first observe that the hysteretic behavior persists as R_V is lowered. In addition, the hysteresis cycle width, $R_M^c - R_M^g$, decreases with R_V. It is interesting to compare their locations with respect to the dynamos windows evidenced in [17, 18] for the Taylor-Green forcing. As shown in Fig. 4, R_M^g values are almost independent of R_V and lie close to the beginning of the first kinematic dynamo mode. Of course, the onset R_M^c switches from the kinematic low branch to the kinematic high branch as R_V increases (and turbulence develops) [17, 18]. The width of the dynamo cycle is thus linked to the evolution of the $R_M^c(R_V)$ curve.

The above results were obtained with a constant force scheme. We have also repeated the quenching procedure using the constant velocity forcing. As can be seen in Fig. 4 (black curve / diamonds symbols), the hysteretic behaviour remains, but the transition towards the non-dynamo state is more abrupt. Another difference concerns the response to quenching; with a constant velocity forcing we observed a lower magnetic saturation level b. Those differences could be explained by a change in hydrodynamics properties such as the fluctuation level, at the same Reynolds number. In addition, when the velocity is kept constant there may be less possibility for the Lorentz force to change the flow.

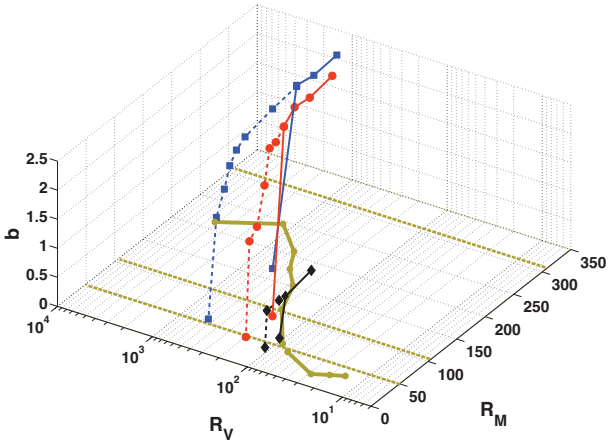

FIG. 4: Hysteresis cycle for different Reynolds numbers and forcings – constant force (red, blue) and constant velocity (black). The thick solid line in the $b = 0$ plane is the linear instability R_M^c *vs* R_V from dynamical runs; the kinematic dynamo windows [18], $R_M \in [50, 110]$ and $R_M > 320$, are delimited by the thick dotted lines.

Finally, we have checked the influence of finite amplitude external perturbations on the hysteresis cycle by applying an external magnetic field of amplitude $B_0 = 0.07$ in the vertical direction. The result at $R_V = 563$ is shown by the blue line in Fig. 2. When comparing to the $B_0 = 0$ case (red curve), two effects are readily observed : (i) the hysteresis cycle is shortened and this is essentially due to a decrease in the onset R_M^c from infinitesimal perturbations; (ii) the amplitude of the magnetic energy in the dynamo is decreased, as lower b values are obtained. These observations are indications that the external magnetic field has mediated a transition towards another equilibrium state [14]. The transition towards this second equilibrium state is quite robust: one can also obtain it by switching on the vertical magnetic field starting from a state with a well-developed dynamo (jump from A to A' in Fig. 2). Conversely, starting from a dynamo state with

an applied magnetic field and switching it off, one returns to the zero-magnetic field hysteresis curve (jump from C to C' in Fig. 2).

A less deterministic behaviour is observed when the system is operated in the vicinity of point D – shown along the blue curve in Fig.2. At this point, the system is operated at a magnetic Reynolds number slightly smaller than the linear threshold (93.8 compared to about 100) and one observes that the the systems spontaneously switches between dynamo and non-dynamo periods, as shown in Fig.5. This is reminiscent of the "on-off" bifurcation scenario sometimes proposed for the dynamo [20, 21, 22, 23] at high R_V. It has been observed in models [24] and experimental [25] versions of the Bullard dynamo [26], and possibly in turbulent fluid dynamos [6]. We note in Fig.5 that the kinetic energy has stronger fluctuations during the dynamo periods.

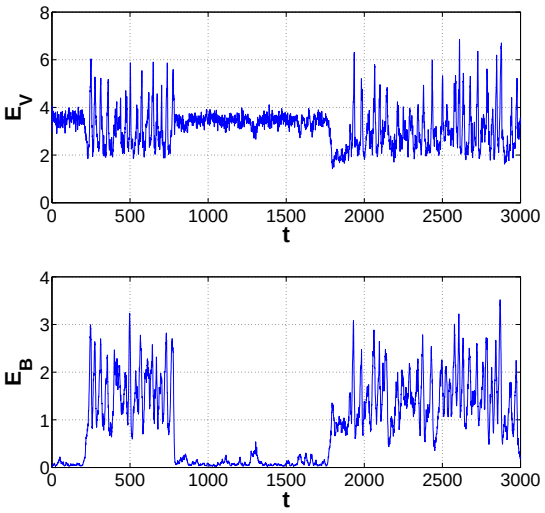

FIG. 5: Evolution on time of the kinetic (E_V) and magnetic energy (E_B) when the flow is operated in the immediate vicinity of point D – see Fig.2.

To summarize, we have evidenced in the TG flow several features characteristic of subcriticality of the dynamo instability. At variance with usual dynamical system, this behaviour is obtained in a fully turbulent system, where fluctuations are of the same order of magnitude as the mean flow. We may remark that in this case, the traditional concept of amplitude equation may be ill-defined and one may have to generalize the notion of 'subcritical transition' for turbulent flows. Another feature is the sensitivity to perturbations of the order parameter through the application of an external magnetic field. The perturbation mainly acts through macroscopic changes in the system configuration (perturbation of the velocity field), allowing lower thresholds for dynamo instability. These findings open new perspective for experimental dynamos. For the TG flow, we observe a decrease of the dynamo threshold by as much as 57 percent, with an external applied field of $B_0 = 0.07$. We have also found that changes in the geometry of the dynamo states in the subcritical branch are consistent with the coexistence of several metastable hydrodynamics states [14]. Preliminary observations in the VKS experiment also point to the existence of subcritical dynamos in the presence of global rotation [27], a feature also noted in some numerical models of the geodynamo [12].

Acknowledgements We acknowledge useful discussions with A. Pouquet and P. Mininni, R. Jover and team members of the VKS collaboration. Computer time was provided by IDRIS and the Mesocentre SIGAMM at Observatoire de la Côte d'Azur. This work is supported by the French GDR Dynamo. YP thanks A. Minuissi for computing design assistance.

[1] J. Larmor, *Rep. Brit. Assoc. Adv. Sci*, 159-160, (1919).
[2] H. K. Moffatt, "Magnetic field generation in electrically conducting fluids", (Cambridge U. Press, 1978);
[3] A. Gailitis et al., *Phys. Rev. Lett.* **86**, 3024 (2001)
[4] R. Stieglitz and U. Müller, *Phys. Fluids* **13** 561 (2001)
[5] R. Monchaux et AD., *Phys. Rev. Lett.* **98** 044502, (2007)
[6] M. Berhanu et al., *Europhys. Lett.* **77**, 59001 (2007)
[7] R. Berthet et al., Physica 174D, 84 (2003)
[8] P. Manneville, "Dissipative Structures and Weak Turbulence", (Academic Press, Boston, 1990)
[9] O. Dauchot, P. Manneville, *J. Phys. II* **7**(2), 371 (1997)
[10] K. A. Robbins, *Proc. Nati. Acad. Sci. USA* **73**(12), 4297-4301 (1976)
[11] S. Fedotov, I. Bashkirtseva and L. Ryashko, *Phys. Rev. E* **73**, 066307 2006.
[12] V. Morin, Ph. D. Thesis, University Paris VI (1999) ; U.R. Christensen, P. Olson and G.A. Glatzmaier, *Geophys. J. Int.*, **138**, 393 (1999).
[13] M. Brachet, *Fluid Dyn. Res.* **8**, 1 (1991); C. Nore et al., *Phys. Plasmas* **4**, 1 (1997)
[14] B. Dubrulle et al, *to appear in NJP* (2007).
[15] A.A. Schekochihin et al., *New J. Physics* **4**, 84 (2002); A.A. Schekochihin et al., *Phys. Rev. Lett.* **92**, 054502 (2004); A. B. Iskakov et al., `arXiv/astro-ph/0702291`
[16] Y. Ponty et al., *Phys. Rev. Lett.* **94**, 164512 (2005)
[17] J.-P. Laval et al., *Phys. Rev. Let.* **96** 204503 (2006)
[18] Y. Ponty et al., *New J. Phys.* (2007)
[19] Imagery using VAPOR code (`www.vapor.ucar.edu`)
[20] S. Lozhkin, D. Sokoloff, P. Frick, *Astronomy Reports* **43**(11), 753 (1999)
[21] D. Sweet et al. *Phys. Rev. E* **63**, 066211 (2001)
[22] N. Leprovost and B. Dubrulle, *Eur. Phys. J. B*, **44** 395 (2005).
[23] M. D. Nornberg et al. *Phys. Rev. Lett.* **97**, 044503 (2006)
[24] N. Leprovost, B. Dubrulle, F. Plunian, *Magnetohydrodynamics* **42**, 131 (2006)
[25] M. Bourgoin et al., *New J. Phys.* **8**, 329, (2006)
[26] E. C. Bullard, *Proc. Camb. Phil. Soc* **51**, 744 (1955)
[27] VKS team, private communication.